RMetS

Royal Meteorological Society

Atmospheric water parameters measured by a ground-based microwave radiometer and compared with the WRF model

Federico Cossu,[1,2]* Klemens Hocke,[1,2] Andrey Martynov,[2,3] Olivia Martius[2,3] and Christian Mätzler[1,2]

[1]*Institute of Applied Physics, University of Bern, Switzerland*
[2]*Oeschger Centre for Climate Change Research, University of Bern, Switzerland*
[3]*Institute of Geography, University of Bern, Switzerland*

Correspondence to:
F. Cossu, Institute of Applied Physics, University of Bern, Sidlerstrasse 5, Bern 3012, Switzerland.
E-mail:
federico.cossu@iap.unibe.ch

Abstract

The microwave radiometer TROWARA measures integrated water vapour (IWV) and integrated cloud liquid water (ILW) at Bern since 1994 with a time resolution of 7 s. In this study, we compare TROWARA measurements with a simulation of summer 2012 in Switzerland performed with the Weather Research and Forecasting (WRF) model. It is found that the WRF model agrees very well with TROWARA's IWV variations with a mean bias of only 0.7 mm. The ILW distribution of the WRF model, although similar in shape to TROWARA's distribution, overestimates the fraction of clear sky periods (83% compared to 60%).

Keywords: microwave radiometer; integrated water vapour; integrated cloud liquid water; WRF model

1. Introduction

The TROpospheric WAter RAdiometer (TROWARA) continuously monitors vertically integrated water vapour (IWV) and vertically integrated cloud liquid water (ILW) at Bern since 1994.

Water vapour and clouds are essential components of the climate system for their role in the water cycle and in the Earth's radiation energy budget. Water vapour, being the most important natural greenhouse gas, contributes to the warming of the atmosphere. Clouds, instead, play a dual role: the cloud droplets, whose mean radius ranges from 4 to 24 μm depending on cloud type (Mason, 1971), reflect the shortwave radiation from the sun (cooling effect) and at the same time they absorb and re-emit the infrared long-wave radiation from the surface (warming effect).

Uncertainties in the representation of cloud processes in climate models explain much of the spread in modelled climate sensitivity, leading to regional errors on cloud radiative effect (CRE) of several tens of watts per square metre (Flato *et al.*, 2013). Komurcu *et al.* (2014) showed that global annual mean fields of cloud liquid water path (LWP, identical to ILW) of six different global climate models (GCMs) can differ by more than a factor of two and that the GCMs' mean LWP is more than two times larger than the highest value observed by satellites.

The fractional coverage of clouds and their liquid water content are two important properties which need to be further investigated in order to understand the biases in CRE in models. A small change of 0.1 mm (1 mm is equal to 1 kg m^{-2}) in ILW produces a variation of several hundred watts per square metre in the downward shortwave flux at the surface (Turner *et al.*, 2007). Given the scarcity of high-quality ground-based cloud liquid water measurements, TROWARA's observations are valuable for a more in-depth analysis of those properties and their comparison with regional climate models (RCMs).

Until now, only TROWARA's water vapour measurements have been considered and a trend analysis study of IWV has been published by Hocke *et al.* (2011). Here we present for the first time TROWARA measurements of integrated cloud liquid water (ILW). The aim of this study is to compare data of IWV and ILW from TROWARA with coincident data from a RCM simulation of summer 2012 in Switzerland performed with the Weather Research and Forecasting (WRF) model.

The outline of this article is as follows. In Section 2, we provide detailed information about TROWARA and the WRF model simulation. In Sections 3 and 4 the time series of IWV and ILW and the characteristics of the statistical distributions of ILW are analysed for TROWARA and for the WRF model. Section 5 contains an outlook on future work. The conclusions about the comparison are presented in Section 6, together with a discussion about the microphysical schemes influence on the WRF model simulation.

2. Data

2.1. TROWARA data

The TROWARA microwave radiometer has been operated at the University of Bern (46.95°N, 7.44°E, 575

m a.s.l.) since 1994. To improve the measurement accuracy during rainy periods, in 2002 TROWARA was moved inside a temperature-controlled room, looking towards southeast through a styrofoam window which is transparent to microwaves. Due to the southeast exposure, most rain events do not deposit any rain on the window. Therefore emission of most rain events can be accurately measured.

The instrument consists of two microwave channels at 21.4 GHz (bandwidth 100 MHz) and 31.5 GHz (bandwidth 200 MHz). The lower frequency is more sensitive to microwave emission from water vapour, while the higher frequency is more sensitive to liquid water. In addition, TROWARA has a channel in the thermal infrared ($\lambda = 9.5 - 11.5 \mu m$) which is required for the estimation of the cloud temperature. The standard elevation angle is 40° and the main lobe of TROWARA's antenna pattern has a full width of 4° at half power.

The measurement principle of TROWARA is based on passive remote sensing of the microwave emission from water vapour and liquid cloud droplets. The zenith opacities at 21 and 31 GHz are derived from the observed brightness temperatures in the two microwave channels. Then, IWV and ILW are derived from a linear combination of the opacities. The retrieval process requires auxiliary information such as surface temperature, pressure and relative humidity which are provided by the local meteorological station.

Compared to the satellite-based microwave radiometers, their surface-based counterparts like TROWARA have the advantage of a well-known cosmic background whose brightness temperature is very isotropic and much less than any atmospheric temperature. Peter and Kämpfer (1992) stated that for TROWARA the error of IWV is about 3% of the measured value. This error is due to the variable water vapour sensitivity of the instrument with altitude. For ILW Peter and Kämpfer (1992) stated an error of 10–20% of the measured value. This error is due to uncertainties in the dielectric constant of water at the unknown cloud temperature. In the currently adopted refined retrieval of Mätzler and Morland (2009), the cloud temperature is estimated using an infrared radiometer, thus reducing the ILW error. Furthermore, progress has been achieved in dielectric models of water (Mätzler *et al.*, 2010). In addition to the percent error, there was a zero bias on the order of 0.01–0.02 mm. Improvements have also been achieved by refined physical retrievals. The present instrument uses a correction to reduce this error to 0.001 mm (Mätzler and Morland, 2009). The remaining uncertainty is limited to rainy conditions when the emission is enhanced by Mie effects.

During rain, the microwave emission of the rain droplets is much larger than that of the cloud droplets. As we are focusing on the estimation of the cloud droplets only (suspended hydrometeors), the emission from the large precipitating hydrometeors (i.e. rain droplets) is a contamination to our measurements.

Therefore, in these conditions, a proper determination of cloud liquid water is not feasible. To overcome this problem, the retrieval algorithm has been designed to allow the user to choose a threshold for ILW, beyond which all further emission is attributed to rain. Mätzler and Morland (2009) found that the presence of rain droplets is likely for ILW values exceeding 0.4 mm (or 0.4 kg m^{-2}). Thus our study concentrates on the analysis of ILW measurements below the threshold of 0.4 mm. We applied the retrieval algorithm to the year 2012 and obtained two time series of IWV and ILW with a time resolution of about 7 s.

2.2. WRF simulation

We performed a simulation of the summer 2012 (June, July and August) in Switzerland with the WRF model version 3.4.1 (Skamarock *et al.*, 2008). The simulation domain extends from 42.72° to 49.91°N and from 4.14° to 12.09°E (Figure S1, Supporting Information) with a horizontal resolution of 2.14 km and 35 vertical levels (top level at 50 hPa). The time step is 4 s and the output is saved every 60 min. The initial state and the update of the boundary conditions (every 6 h) are specified with ECMWF analysis data.

The simulation was repeated using four microphysical schemes to find the scheme which produces the most realistic distributions of water vapour and clouds. The schemes considered in this study are the WRF single-moment 6-class scheme (WSM6) (Hong and Lim, 2006), the new Thompson *et al.* scheme (NT) (Thompson *et al.*, 2008), the Milbrandt-Yau double-moment 7-class scheme (MY) (Milbrandt and Yau, 2005) and the Morrison double-moment scheme (MO) (Morrison *et al.*, 2009). It is known that simulations with the same configuration and initial conditions but with different microphysical schemes can produce different results (Jankov *et al.*, 2005, 2009; Otkin and Greenwald, 2008; Mercader *et al.*, 2010; Awan *et al.*, 2011). A comparison of 13 microphysical schemes for an idealized WRF model simulation can be found in Cossu and Hocke (2014).

For the model comparison with TROWARA measurements, we used the closest grid point to the instrument location (grid point at 46.949°N, 7.432°E). Every microphysical scheme of the WRF model partitions atmospheric water in water vapour and in several hydrometeor classes, such as cloud liquid water, cloud ice, rain droplets and so on. We computed IWV and ILW from the mass mixing ratio vertical profiles of water vapour and cloud liquid water.

3. IWV comparison

Summer months in Switzerland are characterized by the highest amounts of IWV throughout the year which can reach values between 40 and 45 mm. Water vapour is generally transported from the Atlantic Ocean to
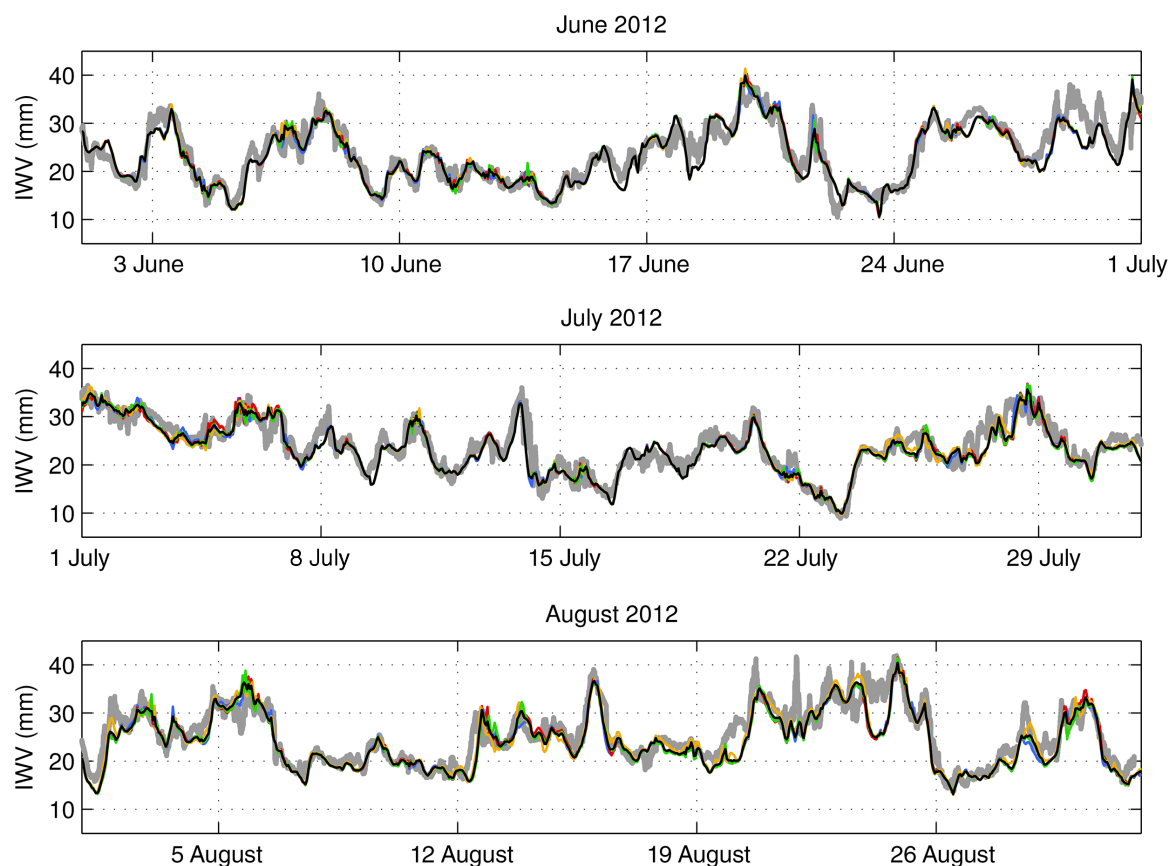
Figure 1. Integrated water vapour (IWV) measured by TROWARA in summer 2012 (grey points) and simulated by the WRF model with four different microphysical schemes (blue, red, yellow and green lines with their mean in black).

Switzerland, but local production of significant quantities of water vapour may occur during hot summer days by evaporation from lakes, rivers, vegetation and moist soil (Sodemann and Zubler, 2010).

Figure 1 shows the time series of IWV measured by TROWARA (grey points) and simulated by the WRF model with the four different microphysical schemes (blue, red, yellow and green lines with their mean in black). TROWARA measurements range from about 9 mm on 23 July to about 42 mm on 24 August with an average of about 24 mm.

The microphysical schemes (WSM6, NT, MY and MO) do not deviate too much from each other. The maximum mean deviation is between MY and MO, with a mean difference IWV_{MY} minus IWV_{MO} of 0.19 mm and a standard deviation of 0.84 mm. The minimum variability between the schemes is found during periods without clouds, for example between 14 and 19 June (a zoom on this period is provided in Figure S2).

The average value of the microphysical schemes, $IWV_{<WRF>}$, follows the TROWARA time series well. The mean difference $IWV_{TROWARA}$ minus $IWV_{<WRF>}$ is 0.7 mm and its standard deviation is 2.3 mm. IWV is simulated with great accuracy being $IWV_{<WRF>}$ on average only 2.4% lower than $IWV_{TROWARA}$.

The good agreement of the model with the measurements can also be seen in the scatter plot of Figure 2, where we show $IWV_{<WRF>}$ versus $IWV_{TROWARA}$. The points above the identity line (overestimation) are shown in magenta colour, while the points below the identity line (underestimation) are shown in cyan colour. The linear regression line is shown in black and has a correlation coefficient of 0.915, indicating the good agreement between the WRF model and TROWARA. The regression line lies for the most part under the identity line, meaning that the underestimation is stronger than the overestimation. By analysing the occurrence times and the coincident ILW values, we found that the overestimation occurs most often in the late evening and in more cloudy conditions (average ILW = 0.062 mm), while the underestimation occurs most often in the early afternoon and in less cloudy conditions (average ILW = 0.025 mm) (occurrence times distributions in Figure S3).

4. ILW comparison

ILW is the vertical integral of the cloud liquid-water content (kg m^{-3}), which depends on the drop size distribution (DSD) of the cloud droplets. Because of the complex microphysical and dynamical processes within clouds, DSDs are highly variable in time and space (Westwater *et al.*, 2005), causing ILW to vary as well. Other processes that determine the variability of DSD and ILW are geographical location and cloud height, local convection and fluxes from the surface, regional and large-scale dynamics.
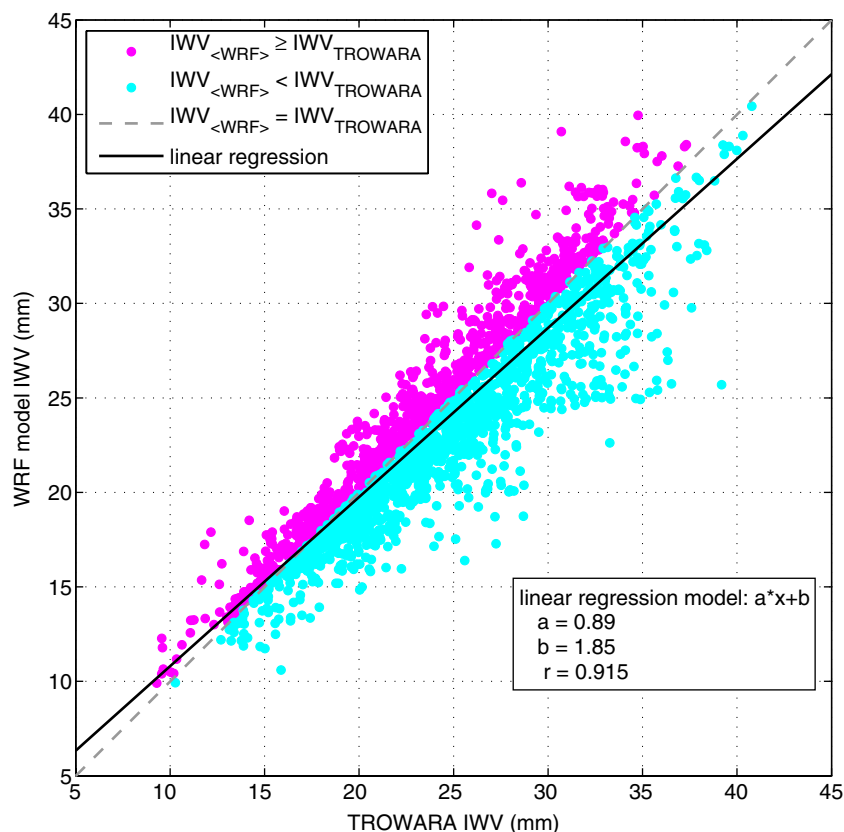
Figure 2. Scatter plot of IWV simulated by the WRF model (average of four different microphysical schemes) versus IWV measured by TROWARA. The dashed grey line is the identity line, the black line is the linear regression line, the magenta points are the cases in which the WRF model overestimates TROWARA measurements and the cyan points the cases of underestimation.

The variability of ILW is larger compared to the variability of IWV. The relative variation of IWV and ILW (computed as the ratio of standard deviation to mean value) for an interval of about 10 min provides a good measure of the variability of the two parameters. For TROWARA measurements in summer 2012, the mean relative variation is about 1% for IWV and about 51% for ILW. The frequency distribution of the relative variation of IWV and ILW is provided in Figure S4.

4.1. Data overview

Figure 3 gives an overview of the ILW data sets of TROWARA and the WRF model and their agreement or disagreement. As for Figure 1, the grey points indicate TROWARA measurements and the coloured lines indicate the four WRF model microphysical schemes with their mean in black. The simulated ILW does not match the radiometer measurements as well as in the case of IWV. The mismatch is caused by the model poor sampling (1 record every hour) and by the difficulty to represent cloud-scale processes in models.

For periods characterized by a more frequent and prolonged occurrence of clouds, as for example between 3 and 14 June, the WRF model performs better, showing a similar probability in the occurrence of clouds to TROWARA. Further, in extended periods dominated by fair weather, as between 14 and 17 June, TROWARA and the WRF model agree in showing no clouds.

Another difference between TROWARA and the WRF model is the range of ILW values. TROWARA values are limited to 0.4 mm, as explained in Section 2.1, while the WRF model values can be higher. The maximum values, which are not displayed in Figure 3, are 1.41 mm (WSM6), 1.49 mm (NT), 2.16 mm (MY) and 3.21 mm (MO).

4.2. ILW distribution

In the following sections we change our focus from the absolute ILW values to their occurrence probability which allows to characterize their distributions. To compute the ILW distributions, we divide the ILW values into three groups: the first group contains the values smaller than 0.01 mm, which represent, ignoring ice clouds (TROWARA is not sensitive to ice particles and we ignored ice clouds in the WRF model as well), clear sky conditions; the second group is subdivided into 10 intervals between 0.01 and 0.4 mm; the third group includes the values greater than or equal to 0.4 mm. The probability of occurrence of each bin is computed by counting the number of values that fall in that bin divided by the total number of points. The computed ILW distributions for TROWARA and for the WRF model are shown in Figure 4.

In summer 2012 at Bern, TROWARA measures a clear sky fraction of 60%, while it is 83% on average for the WRF model simulations. The surplus of clouds
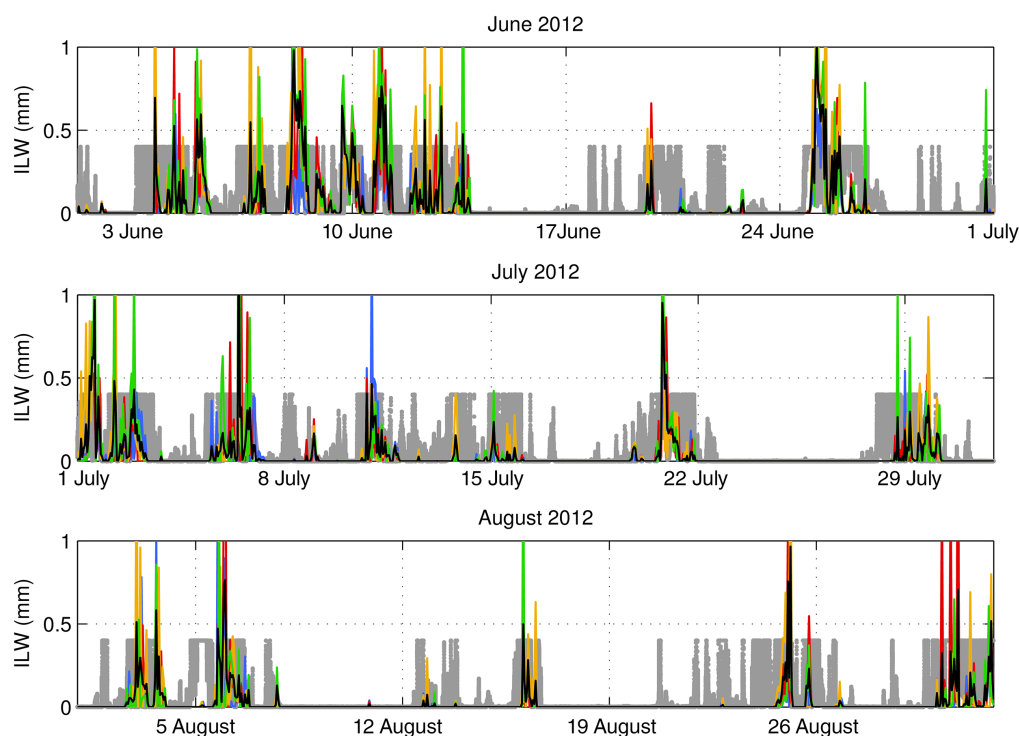
Figure 3. Integrated cloud liquid water (ILW) measured by TROWARA in summer 2012 (grey points) and simulated by the WRF model with four different microphysical schemes (blue, red, yellow and green lines with their mean in black).

in TROWARA data compared to that of the WRF model can also be clearly seen in the time series of Figure 3. There are often periods in which TROWARA measures a positive ILW and the WRF model a null ILW. For these periods, there is an easy way to verify whether TROWARA or WRF is correct by looking at the archive images of the local webcam. A cloudy day is easily recognizable and it would rule out the null ILW value simulated by the WRF model. By looking at the webcam images of the Climate and Environmental Physics Institute of the University of Bern, we could confirm the validity of TROWARA measurements. One of these images is shown in Figure S5.

Between 0.01 and 0.4 mm the ILW distributions of both TROWARA and the WRF model are clearly decreasing, meaning that thick (thin) clouds and/or clouds with a high (low) liquid water content occur less (more) frequently. Owing to the high sensitivity of TROWARA and to the large number of available points, it is possible to increase the binning in this range and to better define the shape of the distribution, as shown in Figure 5. The probability distribution between 0.01 and 0.4 mm seems to follow a power law function and by fitting the data with a two-term power model we obtain the following equation:

$$P(\text{ILW}) = a\text{ILW}^b + c \qquad (0.01 \leq \text{ILW} < 0.4) \quad (1)$$

where $P(\text{ILW})$ is the probability density function of the continuous variable ILW between 0.01 and 0.4 mm, $a = 0.0022$, $b = -0.71$ and $c = -0.0028$. The coefficient of determination R^2 between the measured ILW distribution and the computed probability density function is 0.996, indicating that the ILW distribution in this range resembles well a power law function.

The last bin from 0.4 mm up, albeit having a width of 0.01 mm, includes all the values ≥ 0.4 mm, the threshold value. The occurrence probability of the last bin is lower in the WRF model (0.03 on average) than in TROWARA (0.11) partially because most of the WRF model values are in the first bin, causing the part of the distribution with ILW ≥ 0.01 mm to be lower.

The ILW distribution of the WRF model varies slightly from scheme to scheme and it is similar to TROWARA. In fact, the first bin is the highest one, the bins between 0.01 and 0.4 mm decrease in size and the last bin is higher than the previous ones. A zoom of the occurrence probability between 0 and 0.1 for the WRF model ILW distributions is provided in Figure S6.

There is a substantial difference in the number of points used to compute the distributions of TROWARA and of the WRF model: more than one million points for TROWARA compared to 2209 points for the WRF model. A larger number of points for the WRF model would allow not only to draw more robust statistical conclusions on the clear sky occurrence probability but also to study in more detail the shape of the distribution between 0.01 and 0.4 mm, as done with TROWARA, and to enhance the differences between the microphysical schemes. To increase the number of available points the output frequency must be increased or the simulation period must be extended. It was not possible for us to save the simulation data with such a high frequency because of hard disk space limitations.
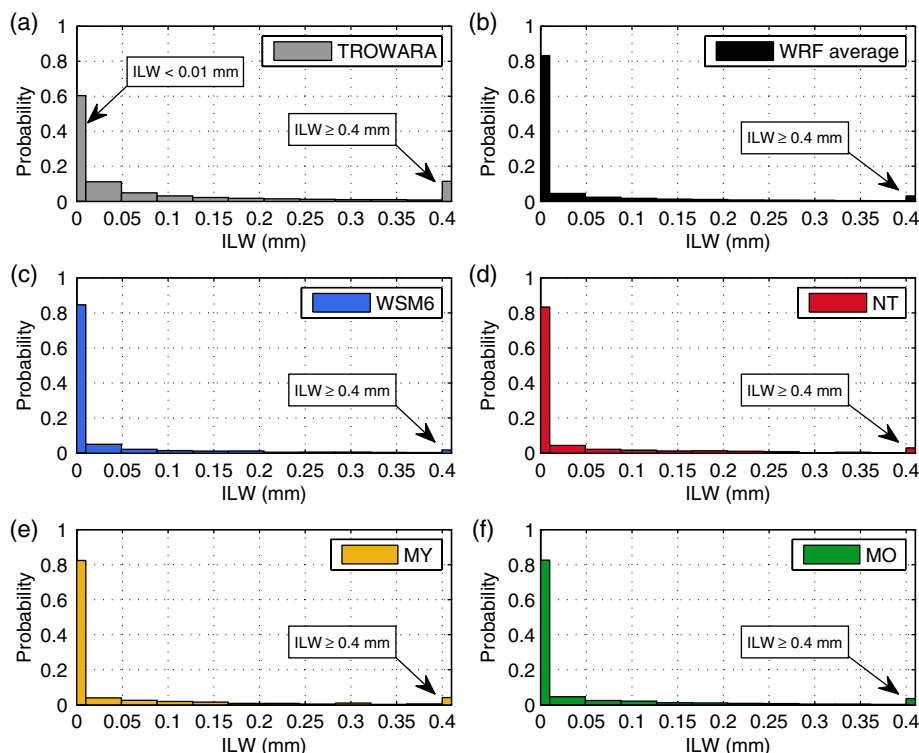
Figure 4. (a) ILW distribution of the values measured by TROWARA in summer 2012. The first bin on the left represents all the values smaller than 0.01 mm (even small negative values), while the last bin on the right represents all the values equal to or greater than 0.4 mm. (b) Average WRF ILW distribution computed by averaging the ILW distributions of the four microphysical schemes. (c–f) ILW distribution of the values simulated by the WRF model using four different microphysical schemes. The last bin on the right in each distribution represents all the values equal to or greater than 0.4 mm.

5. Future work

In future, we will investigate whether the statistics of the simulated ILW can be improved by analysing the output from several model grid-points in the surroundings of Bern. The average ILW distribution of the nearby grid-points could reduce the point-to-point internal variability of the numerical model and improve the model performance at this location.

Simulations with a higher output frequency will allow to better define the shape of the ILW distributions and to enhance the differences between the schemes.

By considering a longer time period, the seasonal behaviour of TROWARA ILW will be analysed to discover possible changes in the clear sky occurrence probability and in the shape of the ILW distribution over the past few years.

Because microwave radiometry is a well established and possibly the most accurate method for retrieving IWV and ILW (Westwater *et al.*, 2005), TROWARA measurements are also valuable for validation of satellite measurements, as in the study of Roebeling *et al.* (2008).

6. Conclusions

In this study, we presented a comparison of IWV and ILW measured in summer 2012 at Bern by the microwave radiometer TROWARA and simulated

with the WRF model using different microphysical parameterizations.

We have found that over a 3-month simulation the WRF model agrees very well with TROWARA's IWV variations. The mean bias $IWV_{TROWARA}$ minus $IWV_{<WRF>}$ is only 0.7 mm and the standard deviation is 2.3 mm. The variation in IWV between the microphysical schemes was minimal and the schemes that differed the most were MY and MO with a maximum mean deviation IWV_{MY} minus IWV_{MO} of 0.19 mm and a standard deviation of 0.84 mm.

For ILW, the main focus of our comparison was on the probability density function of ILW which is especially relevant for climate research, since even small differences in cloud liquid water greatly modify the atmospheric radiative fluxes (Turner *et al.*, 2007). By computing the ILW distributions, we found only a partial agreement between TROWARA and the WRF model. In both ILW distributions the highest occurrence probability is for clear sky periods and the shape of both distributions is gradually decreasing between 0.01 and 0.4 mm. The WRF model, however, overestimates the clear sky fraction (83%) compared to TROWARA (60%).

As in the case of IWV, we did not find substantial differences in the ILW distributions simulated with the selected microphysical schemes. All the four WRF model ILW distributions have in fact almost the same clear sky occurrence probability and a decreasing probability for ILW ≥ 0.01 mm. The relatively small
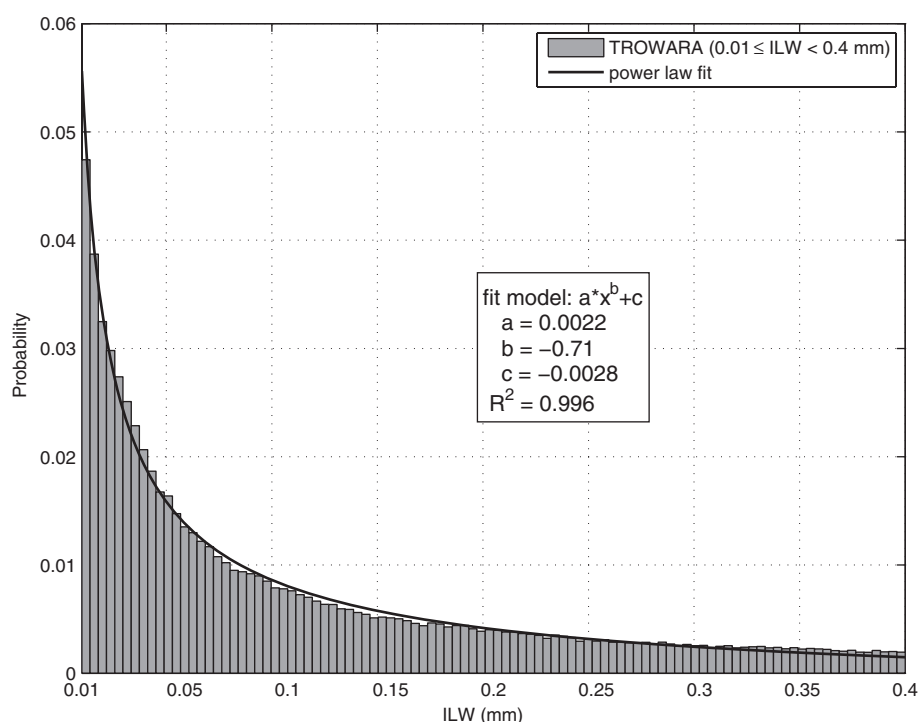
Figure 5. Finer binning and power law fit of the central part of TROWARA ILW distribution between 0.01 and 0.4 mm.

number of available points has however hindered a more detailed comparison of the distributions.

Additionally, we characterized TROWARA's ILW distribution between 0.01 and 0.4 mm, finding that it is well represented by a power law function with an exponent of −0.71 (Equation 1).

Acknowledgements

Supporting information

The following supporting information is available:

Figure S1. The WRF simulation domain extends from 42.72° to 49.91°N and from 4.14° to 12.09°E. The white dot indicates the location of Bern (46.95°N, 7.44°E) where TROWARA is measuring.

Figure S2. IWV variability, expressed as difference between the microphysical schemes (upper panel), is lower during periods without clouds (null ILW, lower panel).

Figure S3. Dependence on local time for the cases in which the WRF model overestimates TROWARA's IWV (upper panel) and for the cases of underestimation (lower panel). The y-axis represents the number of events per hour. The overestimation occurs most often in the late evening, while the underestimation occurs most often in the early afternoon.

Figure S4. Absolute frequency distributions of the relative variations of IWV (top panel) and ILW (bottom panel) measured by TROWARA in summer 2012. The relative variations are computed as the ratio of standard deviation to mean value for intervals of 10 min.

Figure S5. Webcam image from the archive of the Climate and Environmental Physics institute of the University of Bern showing stratus clouds on 24 August 2012 at 0800 UTC. At that time, TROWARA data correctly show a positive ILW value, while the WRF model simulations have a null ILW value. TROWARA is installed near the webcam, pointing in the same direction and with an elevation angle of 40°.

Figure S6. Zoom of the occurrence probability between 0 and 0.1 for the ILW distributions simulated by the WRF model using four different microphysical schemes.

References

Awan NK, Truhetz H, Gobiet A. 2011. Parameterization-induced error characteristics of MM5 and WRF operated in climate mode over the Alpine region: an ensemble-based analysis. *Journal of Climate* **24**: 3107–3123, doi: 10.1175/2011JCLI3674.1.

Cossu F, Hocke K. 2014. Influence of microphysical schemes on atmospheric water in the Weather Research and Forecasting model. *Geoscientific Model Development* **7**: 147–160, doi: 10.5194/gmd-7-147-2014.

Flato G, Marotzke J, Abiodun B, Braconnot P, Chou S, Collins W, Cox P, Driouech F, Emori S, Eyring V, Forest C, Gleckler P, Guilyardi E, Jakob C, Kattsov V, Reason C, Rummukainen M. 2013. Evaluation of climate models. In *Climate Change 2013: The Physical Science Basis. Contribution of Working Group I to the Fifth Assessment Report of the Intergovernmental Panel on Climate Change*, Stocker T, Qin D, Plattner G-K, Tignor M, Allen S, Boschung J, Nauels A, Xia Y, Bex V, Midgley P (eds). Cambridge University Press: Cambridge, UK and New York, NY.

Hocke K, Kämpfer N, Gerber C, Mätzler C. 2011. A complete long-term series of integrated water vapour from ground-based microwave

radiometers. *International Journal of Remote Sensing* **32**: 751–765, doi: 10.1080/01431161.2010.517792.

Hong S-Y, Lim J-OJ. 2006. The WRF single-moment 6-class microphysics scheme (WSM6). *Journal of Korean Meteorological Society* **42**: 129–151.

Jankov I, Gallus WA, Segal M, Shaw B, Koch SE. 2005. The Impact of different WRF model physical parameterizations and their interactions on warm season MCS rainfall. *Weather Forecasting* **20**: 1048–1060, doi: 10.1175/WAF888.1.

Jankov I, Bao J-W, Neiman PJ, Schultz PJ, Yuan H, White AB. 2009. Evaluation and comparison of microphysical algorithms in ARW-WRF model simulations of atmospheric river events affecting the California coast. *Journal of Hydrometeorology* **10**: 847–870, doi: 10.1175/2009JHM1059.1.

Komurcu M, Storelvmo T, Tan I, Lohmann U, Yun Y, Penner JE, Wang Y, Liu X, Takemura T. 2014. Intercomparison of the cloud water phase among global climate models. *Journal of Geophysical Research: Atmospheres* **119**: 3372–3400, doi: 10.1002/2013JD021119.

Mason B. 1971. *The Physics of Clouds*. Oxford Monographs on Meteorology. Clarendon Press: Oxford, UK.

Mätzler C, Morland J. 2009. Refined physical retrieval of integrated water vapor and cloud liquid for microwave radiometer data. *IEEE Transactions on Geoscience and Remote Sensing* **47**: 1585–1594, doi: 10.1109/TGRS.2008.2006984.

Mätzler C, Rosenkranz PW, Cermak J. 2010. Microwave absorption of supercooled clouds and implications for the dielectric properties of water. *Journal of Geophysical Research: Atmospheres (1984–2012)* **115**, doi: 10.1029/2010JD014283.

Mercader J, Codina B, Sairouni A, Cunillera J. 2010. Results of the meteorological model WRF-ARW over Catalonia, using different parameterizations of convection and cloud microphysics. *Journal of Weather and Climate of the Western Mediterranean* **7**: 75–86, doi: 10.3369/tethys.2010.7.07.

Milbrandt J, Yau M. 2005. A multimoment bulk microphysics parameterization. Part I: analysis of the role of the spectral shape parameter. *Journal of the Atmospheric Sciences* **62**: 3051–3064, doi: 10.1175/JAS3534.1.

Morrison H, Thompson G, Tatarskii V. 2009. Impact of cloud microphysics on the development of trailing stratiform precipitation in a simulated squall line: comparison of one- and two-moment schemes.

Monthly Weather Review **137**: 991–1007, doi: 10.1175/2008 MWR2556.1.

Otkin JA, Greenwald TJ. 2008. Comparison of WRF model-simulated and MODIS-derived cloud data. *Monthly Weather Review* **136**: 1957–1970, doi: 10.1175/2007MWR2293.1.

Peter R, Kämpfer N. 1992. Radiometric determination of water vapor and liquid water and its validation with other techniques. *Journal of Geophysical Research: Atmospheres* **97**: 18173–18183, doi: 10.1029/92JD01717.

Roebeling R, Deneke H, Feijt A. 2008. Validation of cloud liquid water path retrievals from SEVIRI using one year of CloudNET observations. *Journal of Applied Meteorology and Climatology* **47**: 206–222, doi: 10.1175/2007JAMC1661.1.

Skamarock W, Klemp J, Dudhia J, Gill D, Barker D, Duda M, Huang XY, Wang W. 2008. A description of the advanced research WRF version 3. Technical report, Mesoscale and Microscale Meteorology Division, National Center for Atmospheric Research, Boulder, CO. http://nldr.library.ucar.edu/repository/collections/TECH-NOTE-000-000-000-855 (accessed 13 December 2012).

Sodemann H, Zubler E. 2010. Seasonal and inter-annual variability of the moisture sources for Alpine precipitation during 1995–2002. *International Journal of Climatology* **30**: 947–961, doi: 10.1002/joc.1932.

Thompson G, Field PR, Rasmussen RM, Hall WD. 2008. Explicit forecasts of winter precipitation using an improved bulk microphysics scheme. Part II: implementation of a new snow parameterization. *Monthly Weather Review* **136**: 5095–5115, doi: 10.1175/2008MWR2387.1.

Turner D, Vogelmann A, Austin R, Barnard J, Cady-Pereira K, Chiu JC, Clough S, Flynn C, Khaiyer M, Liljegren J, Johnson K, Lin B, Long C, Marshak A, Matrosov S, McFarlane S, Miller M, Min Q, Minnis P, O'Hirok W, Wang Z and Wiscombe W. 2007. Thin liquid water clouds: their importance and our challenge. *Bulletin of the American Meteorological Society* **88**: 177–190, doi: 10.1175/BAMS-88-2-177.

Westwater ER, Crewell S, Matzler C. 2005. Surface-based microwave and millimeter wave radiometric remote sensing of the troposphere: a tutorial. *IEEE Geoscience and Remote Sensing Society Newsletter* **134**: 16–33.